Modes of Tropical Variability under Convective Adjustment and the Madden–Julian Oscillation. Part II: Numerical Results

JIA-YUH YU AND J. DAVID NEELIN

Department of Atmospheric Sciences, University of California, Los Angeles, Los Angeles, California

(Manuscript received 18 February 1993, in final form 19 January 1994)

ABSTRACT

Convective interaction with dynamics (CID) dictates the structure and behavior of the eigenmodes of the tropical atmosphere under moist convective adjustment (MCA) when the convective adjustment time scale, τ_c, is much smaller than dynamical time scales, as examined analytically in Part I. Here, the modes are reexamined numerically to include the effects of finite τ_c, again for a primitive equation model with the Betts–Miller MCA parameterization. The numerical results at planetary scales are consistent with the analytical approach, with two well-separated classes of vertical modes: one subset evolves at the cumulus time scale, while the other subset evolves at a time scale set by the large-scale dynamics. All modes are stable for homogeneous basic states in the presence of simple mechanical damping effects. Thus, there is no CISK at any scale under MCA. However, the finite τ_c effect has the property of selectively damping the smallest scales while certain vertical modes at planetary scales decay only slowly. This planetary scale selection contrasts to many linear CISK studies, which tend to select the smallest scale.

The Madden–Julian mode, which resembles the observed tropical intraseasonal oscillation, is found as a single vertical mode arising through Kelvin wave–CID. When the evaporation–wind feedback is included, this slowly decaying MJ mode is selectively destabilized at wavenumber one or two, consistent with the observations in the tropics. Stochastic forcing by nonresolved mesoscale processes can also potentially account for the existence of large-scale tropical variance. When the stochastic forcing occurs in the thermodynamic equation, the propagating deep-convective mode at planetary scales is the most strongly excited. Kinematic forcing excites slowly decaying kinematically dominated modes but cannot account for the characteristics of observed Madden–Julian variance.

1. Introduction

In Part I of this paper (Neelin and Yu 1994, NY hereafter), a linear primitive equation model, linearized about a spatially uniform basic state in radiative–convective equilibrium, with the Betts–Miller (1986) moist convective adjustment (MCA) parameterization has been analyzed to study the modes arising through the interaction between the collective effects of cumulus convection and large-scale dynamics. At the limit of small wavenumber, in which the convective time scale τ_c is a small parameter compared to large-scale evolution times, the analytical approach shows two well-separated regimes of eigenmodes: one class evolves at the convective adjustment time scale and the other class evolves slowly at a time scale set by the large-scale dynamics. Among the slow modes, a single vertical mode is singled out by the thermodynamic constraints that has all the geophysically interesting properties. We refer to this as the "propagating deep-convective mode"; with its slow phase speed and deep structures, it is the most geophysically important of the vertical modes. Among the meridional structures for this propagating deep-convective mode, the Kelvin wave case is striking in its resemblance to the Madden–Julian oscillation (MJO), so we refer to this case as the MJ mode.

This near-adjusted propagating deep-convective mode behaves distinctively compared to the other modes, with structure and eigenvalue determined by convective interaction with dynamics (CID). The dispersion relation leads to a well-defined gross moist stability—which dictates the slow phase speed—and to combined damping effects that lead only to slow decay. Our linear analysis contrasts with many CISK studies in that under MCA there is no CISK. The slow phase speed and deep structures of the propagating deep-convective mode can be attributed to wave CID; the MJ mode can be destabilized only by the inclusion of evaporation–wind feedback.

However, the perturbation expansion in the convective time scale is valid only for sufficiently small wavenumbers, and finite τ_c corrections may dominate when considering higher wavenumber dynamics. Furthermore, while we have seen scale selectivity of the MJ mode due to the radiation boundary condition at cloud top, the impact of the finite τ_c effect on scale selectivity

Corresponding author address: Dr. J. David Neelin, Department of Atmospheric Sciences, University of California, Los Angeles, Los Angeles, CA 90024-1565.
Internet: neelin@nino.atmos.ucla.edu

may be considerable. This question and the detailed calculation of the vertical structures for all modes in the tropical spectrum are most easily addressed by numerical calculation of the eigenvalue problem in finite-difference form. Moreover, a closely related form of the matrix problem can be helpful in determining to what extent the variance spectrum of the tropical troposphere can be accounted for by noise arising from nonresolved mesoscale processes exciting large-scale weakly damped modes. In addition to providing a framework for understanding the behavior of GCMs using MCA parameterizations and for contrasting the behavior of cumulus parameterizations in a large-scale context, we hope this will give insight into the origins of large-scale tropical perturbations.

In section 2, the basic equations and the formulation of the eigenvalue problem are stated along with a linearized version of the Betts–Miller parameterization in finite-difference form. Section 3 discusses the general behavior of eigenmodes, focusing on scale selectivity introduced by the finite τ_c effect. Section 4 presents the regimes of eigenmode behavior, including "kinematically dominated modes," "moisture modes," "quasi-dry modes," and "stationary deep-convective mode." The propagating deep-convective mode, due to its strong physical significance, is discussed separately in section 5, focusing on dynamics of the MJO and the evaporation–wind feedback. In section 6, a slightly variant form of the eigenvalue problem is used to study the impact of nonresolved stochastic forcing. Summary and discussion are then given in section 7. A preliminary assessment of the impact of the midlatitude perturbations on the moist tropical waves is presented in the appendix.

2. Formulation of eigenvalue problem

a. Basic equations

In NY, we have assumed a long-wave approximation to simplify the eigenvalue problem and make the analytical approach tractable. Here we initially consider the case without the long-wave assumption and qualitatively discuss the resulting eigenvalue problems for short Rossby waves and mixed Rossby–gravity waves. The ω equation, thermodynamic equations, and moisture equations for the troposphere and boundary layer (PBL) are

$$\partial_p^2\omega' + \frac{R}{p}\mathscr{L}_{\lambda,k,y}T' = 0, \tag{2.1a}$$

$$(\lambda + \epsilon_r)T' + \frac{1}{C_p}(\partial_p\bar{S})\omega' = Q_c'(T', q', T_b', q_b', \bar{T}), \tag{2.1b}$$

$$\lambda q' + (\partial_p\bar{q})\omega' = Q_q'(T', q', \bar{T}), \tag{2.1c}$$

$$(\lambda + \epsilon_b)T_b' + \frac{1}{C_p}(\Delta\bar{S}_b/\Delta p_b)\omega_b' = Q_c'(T', q', T_b', q_b', \bar{T}), \tag{2.1d}$$

$$\lambda q_b' + (\Delta\bar{q}_b/\Delta p_b)\omega_b' = Q_q'(T_b', q_b', \bar{T}) + E'(\Delta p_b/g)^{-1}. \tag{2.1e}$$

The operator $\mathscr{L}_{\lambda,k,y}$ in (2.1a) is defined as

$$\mathscr{L}_{\lambda,k,y} = \frac{(\lambda + \epsilon_m)}{[(\lambda + \epsilon_m)^2 + \beta^2y^2]}\partial_y^2 - \frac{2\beta^2y(\lambda + \epsilon_m)}{[(\lambda + \epsilon_m)^2 + \beta^2y^2]^2}\partial_y - \left\{\frac{ik\beta + k^2(\lambda + \epsilon_m)}{[(\lambda + \epsilon_m)^2 + \beta^2y^2]} - \frac{2ik\beta^3y^2}{[(\lambda + \epsilon_m)^2 + \beta^2y^2]^2}\right\}, \tag{2.1f}$$

where k is the wavenumber and λ is again the eigenvalue with the real part denoting growth rate and the imaginary part denoting frequency. All the variables and constants are the same as those in NY. We note for reference that Q_c', Q_q', and E' denote, respectively, the convective heating, moisture source, and evaporation perturbations; $\Delta\bar{S}_b$ and $\Delta\bar{q}_b$ denote the jumps of dry static energy and specific humidity between boundary layer and the troposphere; $\partial_p\bar{S}$ and $\partial_p\bar{q}$ denote, respectively, the dry static energy stratification and specific humidity stratification in the troposphere; ϵ_r is the radiative cooling rate, and ϵ_m the momentum damping rate; subscript b denotes boundary-layer variables, and Δp_b is the pressure depth of the boundary layer. With parameterizations of cumulus convection (Q_c' and Q_q') and evaporation (E'), along with suitable y boundary conditions, (2.1a–e) are a complete set of equations for the two-dimensional eigenvalue problem in y and p.

For the same separable case as considered in NY, if ϵ_r, ϵ_m, $\partial_p\bar{S}$, and $\partial_p\bar{q}$ are all independent of y, (2.1a) can be consistently separated into

$$\partial_p^2\omega' + \frac{(\lambda + \epsilon_m)}{c^2}\frac{R}{p}T' = 0 \tag{2.2a}$$

with

$$\partial_y^2Y(y) - \frac{2\beta^2y}{(\lambda + \epsilon_m)^2 + \beta^2y^2}\partial_yY(y) + \left\{\frac{ik\beta}{(\lambda + \epsilon_m)}\left[\frac{\beta^2y^2 - (\lambda + \epsilon_m)^2}{(\lambda + \epsilon_m)^2 + \beta^2y^2}\right] - k^2 - \frac{(\lambda + \epsilon_m)^2 + \beta^2y^2}{c^2}\right\}Y(y) = 0, \tag{2.2b}$$

where $Y(y)$ is the horizontal structure function and c^2 is the separation constant. The horizontal structure equation (2.2b), with decaying boundary conditions at a very large distance from the equator, gives the following dispersion relations (Matsuno 1966):

$$\lambda + \epsilon_m = -ikc, \quad \text{for} \quad n = -1 \tag{2.3a}$$

$$(\lambda + \epsilon_m)^3 + (\lambda + \epsilon_m)[(2n + 1)\beta c + k^2c^2] - i\beta kc^2 = 0, \quad \text{for} \quad n \geqslant 0, \tag{2.3b}$$

where (2.3a) is the dispersion relation for Kelvin wave ($n = -1$). Equation (2.3b) contains three roots of λ for a given pair of $n(\neq 0)$ and k. They are

$$\lambda + \epsilon_m = \frac{ikc}{(2n + 1) + k^2c/\beta} \tag{2.4a}$$

and

$$\lambda + \epsilon_m = \pm ikc\left[1 + \frac{(2n + 1)\beta}{k^2c}\right]^{1/2}, \tag{2.4b}$$

where (2.4a) is a set of low-frequency westward propagating Rossby waves and (2.4b) denotes a set of westward and eastward propagating inertial–gravity waves. Also, there are two special solutions with $n = 0$, that is,

$$\lambda + \epsilon_m = ikc\left[-\frac{1}{2} \pm \left(\frac{1}{4} + \frac{\beta}{ck^2}\right)^{1/2}\right], \tag{2.4c}$$

where the low-frequency mode is the westward propagating mixed Rossby–gravity wave and the high-frequency mode is the eastward propagating inertial–gravity wave.

We note that the behavior of vertical structure for different meridional modes is sensitive to the choice of cumulus parameterization scheme and it is not necessary that all the tropical waves have the same vertical structure equation. Considering the inviscid case, (2.2a) and (2.1b) can be combined into a single vertical structure equation,

$$c^2\partial_p^2\omega' - \kappa(\partial_p\bar{S}/p)\omega' = -Q_c', \tag{2.5}$$

where $\kappa = R/C_p$. For those cumulus parameterizations with $Q_c = Q_c(\omega)$, like Kuo-type schemes (Kuo 1965, 1974), (2.5) is uniquely solvable with c^2 as the eigenvalue independent of λ. Thus, all the tropical waves share the same vertical structure equation and all the meridional modes can be derived once c^2 is known. However, for those schemes in which the collective effect of cumulus convection is parameterized through thermodynamic variables, like the moist convective adjustment (MCA) scheme (Manabe 1965; Betts 1986), (2.5) is no longer closed, and we must include thermodynamic and moisture equations to get a complete system for the vertical structures.

In our case, the system is most conveniently solved by substituting the relation between c and λ from the horizontal structure equations, (2.3a) and (2.4a–c), into the vertical structure equations and solving the latter for λ. In general, this results in a nonlinear eigenvalue problem. A system linear in λ in standard form results for the vertical structure equations of the Kelvin wave, short inertial–gravity waves, and long Rossby waves. With the aid of (2.3a), (2.4a), and (2.4b), all three cases can be expressed handily as

$$(\lambda + \epsilon_m)\partial_p^2\omega' - \frac{k^2}{(2n + 1)^2}\frac{R}{p}T' = 0, \tag{2.6}$$

where the case $n = -1$ corresponds to the Kelvin wave (or, with k reinterpreted, to short inertial–gravity waves) and $n = 1, 2, \cdots$ denotes the nth long Rossby wave. The identity of the vertical structure for the Kelvin wave and long Rossby waves is handy: the dispersion diagram and eigenmode vertical structures as a function of k are identical except that k^2 is modified by a factor of $(2n + 1)^{-2}$ for the Rossby modes. For long inertial–gravity waves, short Rossby waves, and mixed Rossby–gravity waves, however, the dependence of the latent heating and moistening upon thermodynamic variables in MCA leads to a much more complicated nonlinear eigenvalue problem. For example, with the aid of (2.4a), the vertical structure equation of the short Rossby waves is

$$(\lambda + \epsilon_m)\partial_p^2\omega' - \frac{[1 + 2i(\lambda + \epsilon_m)k/\beta - (\lambda + \epsilon_m)^2k^2/\beta^2]}{(2n + 1)^2} \times \frac{R}{p}k^2T' = 0; \tag{2.7a}$$

while for the mixed Rossby–gravity wave, it is

$$(\lambda + \epsilon_m)\partial_p^2\omega' + \left[\frac{\beta^2}{k^2(\lambda + \epsilon_m)^2} + \frac{2i\beta}{k(\lambda + \epsilon_m)} - 1\right] \times \frac{R}{p}k^2T' = 0. \tag{2.7b}$$

b. Parameterization of cumulus convection

We have discussed, in NY, the physical background of the Betts–Miller MCA scheme (Betts 1986; Betts and Miller 1986) and the selected reference profiles. Here, we present only elements of the cumulus parameterization necessary for the formulation of the eigenvalue problem. Following the Betts parameterization for deep convection, the closure assumptions on latent heating, moisture source, and column energy conservation constraint are

$$Q_c' = \epsilon_c(T_c' - T' - \Delta T_c'), \tag{2.8a}$$

$$Q_q' = \epsilon_c(q_c' - q'), \tag{2.8b}$$

$$C_p \int_{p_T}^{p_0} Q_c' \frac{dp}{g} = -L \int_{p_T}^{p_0} Q_q' \frac{dp}{g}, \qquad (2.8c)$$

where T_c' and q_c' are the temperature and specific humidity reference profiles toward which the scheme adjusts. The levels p_T and p_0 are, respectively, cloud top and cloud base; $\Delta T_c'$ is a correction to the reference profile to satisfy the energy conservation constraint; and $\epsilon_c = \tau_c^{-1}$ is the inverse of the relaxation time scale of cumulus convection.

The reference profile of specific humidity is a given fraction of subsaturation, $\alpha(p)$, that is, $Lq_c' = \alpha\gamma C_p T'$, with $\gamma = d(Lq_{\text{sat}})/d(C_pT)|_{\bar{T}}$, where q_{sat} is the saturation specific humidity. The perturbation temperature reference profile is given by the moist adiabat rising from PBL through the depth unstable to deep convection, that is, by

$$C_pT_c' + \phi_c' + Lq_{\text{sat}}'(\bar{T}, T_c') = C_pT_b' + \phi_b' + Lq_b'. \qquad (2.9)$$

This can be expressed either recursively, using a staggered grid in the vertical with ϕ carried at the half-integer levels and ω, T carried at the integer levels (Fig. 1), as

$$C_pT_{c,k}' = \frac{1}{\left(1 + \frac{1}{2}a_k + \gamma_k\right)}\Big[-\sum_{j=k+1}^{K-1} a_j C_p T_{c,j}' + (1 - a_K)C_pT_b' + Lq_b'\Big], \qquad (2.10)$$

where K denotes the index of cloud-base level and $T_{c,k}'$ stands for perturbation temperature reference profile, T_c', at kth level with $a_j = \kappa(\ln p_{j+1/2} - \ln p_{j-1/2})$; or as

$$C_pT_{c,k}' = A_k(C_pT_b' + Lq_b'), \qquad (2.11)$$

where A_k is a discretized approximation to

$$A(p) = \frac{1}{(1+\gamma)} \exp\left[-\kappa \int_p^{p_b} \frac{1}{(1+\gamma)}\, d\ln p\right]. \qquad (2.12)$$

Thus, the temperature reference profile of deep convection can be expressed as a vertically weighted function of large-scale boundary-layer thermodynamic variables, T_b' and q_b'. Figure 2 shows the weighting profile, $A(p)$, calculated from an observed temperature sounding in the tropics. The vertical dependence of the temperature reference profile is completely determined by γ, which depends only on basic-state temperature; if the subsaturation parameter α does not vary strongly with height, then γ also strongly controls the moisture reference profile. However, we note that for modes under convective adjustment, the Q_c' and Q_q' profiles are not closely linked to the reference profiles but rather are determined internally by the interaction of the convective constraints with the large-scale dynamics.

The temperature reference profile is also constructed to satisfy the enthalpy constraint, (2.8c), which gives a temperature correction term,

$$C_p\Delta T_c' = \frac{1}{\Delta p_T}\left[\int_{p_T}^{p_b} C_p(T_c' - T')dp + \int_{p_T}^{p_b} L(q_c' - q')dp\right]. \qquad (2.13a)$$

With the aid of (2.11), (2.13a) yields

$$C_p\Delta T_c' = A_1C_pT_b' + A_2Lq_b' - \frac{L}{\Delta p_T}\sum_{k=1}^{K-1} q_k'\Delta p_k - \frac{C_p}{\Delta p_T}\Big(\sum_{k=1}^{K-1} T_k'\Delta p_k - \sum_{k=1}^{K-1}\alpha_k\gamma_k T_k'\Delta p_k\Big), \qquad (2.13b)$$

where the unitless constants A_1, A_2 are defined as

$$A_1 = \frac{1}{\Delta p_T}\sum_{k=1}^{K-1} A_k\Delta p_k + \frac{\Delta p_b}{\Delta p_T}\alpha_b\gamma_b,$$

$$A_2 = \frac{1}{\Delta p_T}\sum_{k=1}^{K-1} A_k\Delta p_k - \frac{\Delta p_b}{\Delta p_T}.$$

Here Δp_T is the total length of the column over which convective heating applies and $k = 1$ is the index of cloud-top level. This constant energy correction is applied to each level in the heating region from cloud base to cloud top and will give terms for each T_k, q_k, T_b, and q_b in the matrix **A** of (2.15), in each thermodynamic equation.

In the analytical results (NY), there was little qualitative difference between the rigid-lid condition and the radiation upper boundary condition for the dispersion relation of the MJ mode, except that the small correction due to the radiation condition could further stabilize smaller scales and retard the phase speed. In numerical results, we use a rigid-lid boundary condition for two reasons: (i) it greatly simplifies the solution method, and (ii) to test the effects of scale selectivity due purely to finite τ_c effects. The vertical boundary conditions are just

$$\omega'(p_T) = \omega'(p_0) = 0. \qquad (2.14)$$

We use the vertical structure equations (2.6) and (2.1b–e), which apply uniformly for all scales for the Kelvin meridional mode. The same equations apply to short gravity waves and, with suitable rescaling of zonal wavenumber, to the long Rossby waves. Thus, our discussion, for instance, of the MJ mode provides a prototype for other meridional versions of propagating

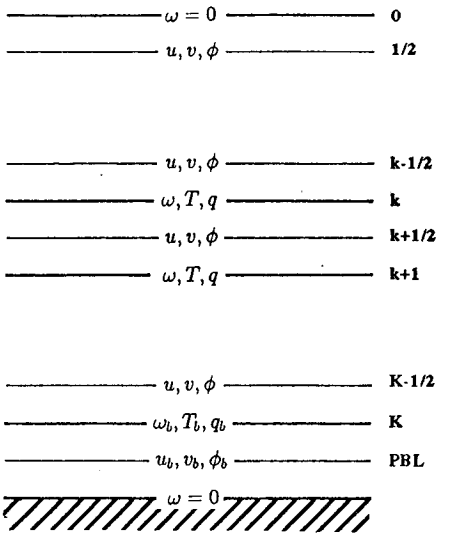

FIG. 1. The vertically staggered grid used in this model.

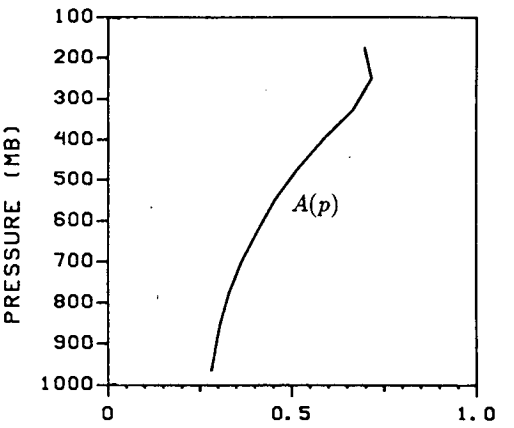

FIG. 2. $A(p)$, the vertical dependence of the temperature reference profile.

deep-convective modes. This system, (2.1b–e) and (2.6), thus becomes a standard eigenvalue problem for the growth rate/frequency, λ, of the form:

$$\lambda \mathbf{BX} = \mathbf{AX}, \tag{2.15}$$

where **X** is the eigenvector, which includes ω, T, and q at all levels; and **A** and **B** are $3N \times 3N$ square matrices with N denoting total vertical levels in the model. In our numerical calculations, $N = 12$ (fairly typical of GCM resolution in the troposphere) is used to resolve the vertical structure of eigenmodes, using the staggered grid shown in Fig. 1 with equal pressure increments of 75 mb.

The heating term, $(T_c' - T')/\tau_c$, must be zero above cloud top, and the level of cloud top should be determined by where the moist adiabat intersects the ambient temperature. Neglecting the perturbation due to cloud top, we simply estimate climatological cloud top from $\overline{\hat{h}_{\text{sat}}} = \overline{\hat{h}_b}$. Taking cloud base to be at 925 mb, from Fig. 1 of NY, the cloud top is estimated to occur within the 100–175-mb layer. While the basic state is, by the horizontal homogeneity assumption, in radiative-convective equilibrium, we do not explicitly solve a radiative-convective model but rather use a representative tropical sounding as in Part I. This allows us to distinguish the implications of the convective scheme and its parameters for the perturbation evolution from the effects that these might have upon the basic state. The implied basic-state radiative term could be diagnosed if desired. Table 1 lists the magnitudes of parameters used in the numerical calculation for the standard case.

3. General behavior of eigenmodes—The finite τ_c effect

The evaporation–wind feedback mechanism is neglected at first for the purpose of isolating the physical processes associated purely with CID. Figure 3a shows the growth rates of all vertical modes as a function of wavenumber for the Kelvin meridional mode. We note that all modes are stable for all wavenumbers in the presence of damping effects. At low wavenumbers, the decay rates are well separated into fast modes, decaying at or near the cumulus time scale, τ_c, and slow modes, decaying at the mechanical damping time scale or slower as discussed in the analytical approach (NY). This separation persists qualitatively to wavenumbers on the order of 20, although deviations begin to occur even at lower wavenumbers. We refer to this regime of behavior, in which the smallness of τ_c strongly constrains the dynamics, as the "planetary-scale regime."

On the other hand, at high wavenumbers, of order 75 or larger, groups of eigenvalues may be found that have, respectively, slow decay rates, decay times of around $2\tau_c$, and decay times of around τ_c. For these modes, τ_c is no longer small compared to the time scales typical of the dynamics. We refer to this regime of behavior as the "smaller-scale regime." We note

TABLE 1. Magnitude of the constants and parameters used in this paper.

Parameter	Symbol	Value
Cumulus relaxation time	τ_c	2 hours
Subsaturation constant	α	0.8
Mechanical damping rate	ϵ_m	$(10 \text{ days})^{-1}$
Radiative damping rate	ϵ_r	$(10 \text{ days})^{-1}$
PBL thermal damping rate	ϵ_b	$(2 \text{ days})^{-1}$
PBL moisture damping rate	ϵ_q	$(1 \text{ day})^{-1}$
Sea level pressure	p_0	1000 mb
Cloud-base pressure	p_b	925 mb
Cloud-top pressure	p_T	100 mb
Vertical grid space	Δp	75 mb
PBL pressure depth	Δp_b	75 mb
Saturation vapor pressure at 25°C	e_0	31.667 mb
Basic-state surface temperature	$\bar{T}_0$	298.2 K
Basic-state PBL specific humidity	$\bar{q}_b$	18 g kg^{-1}

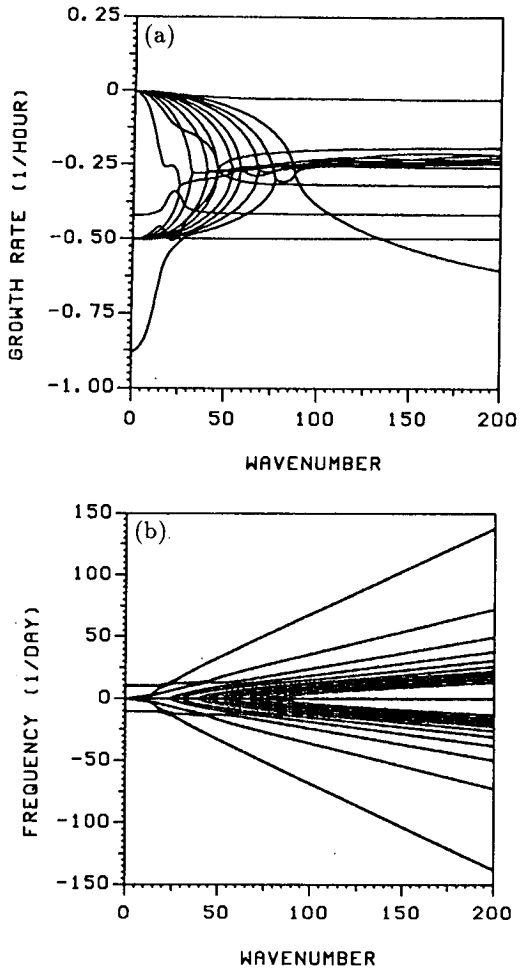

FIG. 3. Eigenvalues of all vertical modes as a function of zonal wavenumber: (a) growth rate as a function of wavenumber and (b) frequency as a function of wavenumber.

that MCA may not necessarily be the best representation of cumulus effects at wavenumbers approaching the mesoscale, but it is of interest to understand the overall behavior of the scheme as a function of scale.

Between these two regimes is a gradual transition in which almost all the modes that were slowly decaying in the planetary regime become much more strongly damped. This scale selectivity is due to the finite τ_c effect [compare with the analytical theory (NY) in which no scale selectivity occurs in the rigid-lid case]. We will discuss two aspects of this selective damping of smaller scales: the implication for planetary-scale selection in the MJO (section 5) and the numerical implications for removing spurious solutions at short scales (section 4). In the transition between the regimes, pairs of modes from the slow and fast decaying branches, respectively, merge to a complex conjugate pair with a decay time of around $2\tau_c$. These complex pairs correspond to propagating waves with frequency as shown in Fig. 3b. For higher wavenumbers, they become nearly nondispersive, while the decay rate remains constant.

There are two subclasses of vertical modes that behave distinctively compared to the others in Fig. 3a, with eigenvalues that are not strongly affected by the finite τ_c effect. Both consist of purely decaying modes: one has slow decay rate even at high wavenumbers; the others decay at the convective time scale for all wavenumbers. The classification of most of the above eigenmodes is given in section 4 to assist qualitative interpretation of the behavior of GCMs using convective adjustment schemes. The propagating deep convective mode, a single mode embedded in the slow modes, is discussed separately in section 5, due to its great geophysical significance.

Figure 3 gives the Kelvin wave case for $\tau_c = 2$ hours. Since the regimes of behavior depend on the relative time scales of the large-scale dynamics and τ_c, changing τ_c essentially has the effect of rescaling wavenumber. Aside from effects of thermodynamic damping terms, changing τ_c by a factor of δ rescales k in Fig. 3 by a factor of $\delta^{-1/2}$ and λ by a factor of δ^{-1}, that is, the transition from the planetary-scale regime occurs at a smaller wavenumber for a larger value of τ_c. The scale selectivity due to τ_c thus increases for larger τ_c. Since τ_c represents the characteristic time scale with which convection removes convective available potential energy from the column at the subgrid scale, it is reasonable to imagine that organization of cumulus convection by subgrid mesoscale motions might have a gross effect similar to increasing τ_c. The τ_c dependence given here may thus be of use to GCM modelers interested in sensitivity to this parameter.

4. Classes of eigenmode in planetary and smaller-scale regimes

Table 2 summarizes the classes of vertical modes found at wavenumber one. This is the archetypical case in the planetary-scale regime, in which τ_c is small compared to large-scale dynamical time scales. To facilitate comparison of the physical character of the eigenmodes, the nondimensional ratios that provide a measure of T amplitude relative to ω amplitude and q amplitude relative to ω amplitude are given. Specifically, the root-mean-square of all T or q elements of the eigenvector are compared to the root-mean-square of all ω elements. These ratios are nondimensionalized by a constant, chosen such that the ratios for the propagating deep-convective mode are order unity. Since T and q were in energy units, the same constant is applied in all cases. Among the slow modes, these ratios and the frequency clearly distinguish between the "propagating deep-convective mode," with intraseasonal time scale, and a second subclass, the "kinematically dominated modes."

Among the fast modes, three subclasses may be distinguished. The largest subclass has eigenvectors dominated by the moisture component, which we thus refer

TABLE 2. Eigenvalues and classification of eigenmodes at wavenumber one, where $\mathscr{C}$ is a constant chosen such that the ratios measuring relative amplitude of T, q, and ω are nondimensional. For brevity, q denotes the moisture modes, DA denotes the deep-adjustment modes, PDC denotes the propagating deep-convective modes, and KD denotes the kinematically dominated modes. "Number" denotes the number of modes in each subclass arising from the eigenvalue problem with N vertical levels before elimination of modes by meridional boundary conditions. Em-dashes in the "period" column denote nonoscillatory modes.

Decay rate	Period	$\mathscr{C}(\Sigma T_i^2/\Sigma\omega_i^2)$	$\mathscr{C}(\Sigma q_i^2/\Sigma\omega_i^2)$	Subclass	Number
		Slow modes			
$(10.8\text{ days})^{-1}$	33.8 days	O (10^0)	O (10^0)	PDC	2
$(9.9\text{ days})^{-1}$	—	O (10^{-4})	O (10^{-2})		
$(9.8\text{ days})^{-1}$	—	O (10^{-3})	O (10^{-2})	KD	$N-1$
⋮	—	⋮	⋮		
		Fast modes			
$(2.15\text{ hours})^{-1}$	13.5 hours	O (10^3)	O (10^3)	Other	2
$(1.99\text{ hours})^{-1}$	—	O (10^3)	O (10^9)		
$(1.98\text{ hours})^{-1}$	—	O (10^4)	O (10^7)	q	$2N-4$
⋮	—	⋮	⋮		
$(1.40\text{ hours})^{-1}$	—	O (10^3)	O (10^3)	DA	1

to as the "moisture modes." The other two subclasses consist of only one mode or one complex pair. Both types were found in NY to obey special balances. The one with complex eigenvalue (propagating waves) has a period of about a half-day. This mode could potentially cause numerical problems with GCMs running MCA due to its high phase speed, although this occurs only at planetary scales since the frequency is almost independent of wavenumber. What would happen to this mode under various discretization schemes is unclear. The mode with stationary decay, faster than the cumulus adjustment time, has a deep heating profile and thermodynamic balances between moisture decay balanced by precipitation and latent heating balanced by temperature increase. We refer to this as the "deep-adjustment mode." We note that these vertical modes in the planetary-scale regime are consistent with the analytical approach (NY), even though some of the fast modes were not fully understood.

Table 3 summarizes classes of vertical modes found at wavenumber 100, as a typical case in the smaller-scale regime, in which τ_c is no longer small compared to the characteristic time scales of the dynamics. We find that only half of the moisture modes carry over to the smaller-scale regime; the other half merge with the kinematically dominated modes to become complex conjugate pairs (propagating waves). These modes have properties similar to the internal modes caused by

TABLE 3. As in Table 2 except for eigenvalues at wavenumber 100. Subclass QD denotes the quasi-dry modes and SDC denotes the stationary deep-convective mode. Em-dashes in the "phase speed" column denote nonoscillatory modes; phase speeds rather than periods are given since oscillatory quasi-dry modes are almost nondispersive at high wavenumbers.

Decay rate	Phase speed	$\mathscr{C}(\Sigma T_i^2/\Sigma\omega_i^2)$	$\mathscr{C}(\Sigma q_i^2/\Sigma\omega_i^2)$	Subclass	Number
		Slow modes			
$(1.5\text{ days})^{-1}$	—	O (10^{-7})	O (10^{-2})	SDC	1
		Fast modes			
$(4.9\text{ hours})^{-1}$	166 m s^{-1}	O (10^{-3})	O (10^{-2})		
⋮	⋮	⋮	⋮		
$(4.0\text{ hours})^{-1}$	43 m s^{-1}	O (10^{-2})	O (10^{-2})	QD	$2N+1$
⋮	⋮	⋮	⋮		
$(3.9\text{ hours})^{-1}$	28 m s^{-1}	O (10^{-3})	O (10^{-2})		
$(1.99\text{ hours})^{-1}$	—	O (10^{-3})	O (10^5)		
$(1.98\text{ hours})^{-1}$	—	O (10^{-3})	O (10^5)	q	$N-2$
⋮	—	⋮	⋮		

the lid condition in the dry atmosphere so we refer to them as the "quasi-dry modes." There is also one stationary mode that has a slow decay rate even at high wavenumbers. This stationary mode has a deep convective structure so we refer to this as the "stationary deep-convective mode."

a. Kinematically dominated modes

At low wavenumbers, the kinematically dominated modes comprise about one-third of the vertical modes (Table 2) and decay slowly at the mechanical damping time. The decay rates of these modes tend to merge with half of the moisture modes at high wavenumbers to become complex conjugate (propagating waves), as shown in Fig. 3a. For wavenumbers above these mergers, they become quasi-dry modes. The transition between these is gradual, so the reasons for the merger can be partially discussed from quasi–dry dynamics (see section 4c). Figure 4 shows the energy and moisture budgets of a typical kinematically dominated mode at wavenumber one, where $\lambda \approx -\epsilon_m$. The energy (moisture) balance of these modes is exactly between adiabatic cooling (moisture convergence) and latent heating (moisture source). Also as described in analytical theory, the vertical velocity has significant amplitude in the upper level when vertical velocity at cloud base is nonzero. The vertical velocity wiggles about a mean value since these modes inherit part of their dynamics from dry internal modes—this creates the irregular vertical structure seen in Fig. 4. The discreteness of the kinematically dominated modes, as for the quasi–dry modes, is associated with the lid condition at the top. Happily, these modes have larger decay rates at higher wavenumbers, due to the finite τ_c effect. This scale selectivity is a nice property since the short waves, which are often poorly represented and are potentially a source of spurious instability in the numerical integration, are more rapidly decaying under MCA. When Rayleigh friction is replaced with vertical diffusion, these modes will decay at rates associated with the vertical diffusion operator. This will split the near degeneracy of the eigenvalues at low wavenumbers, replacing the decay rate ϵ_m with a sequence of decay rates that increase for modes with higher vertical wavenumbers.

b. Moisture modes

At low wavenumbers, two-thirds of the vertical modes are dominated by the moisture component. Half of them have near-constant, fast decay rates at the convective time scale for all wavenumbers. The other half have wavenumber-dependent decay rates, which tend to merge with the kinematically dominated modes at higher wavenumbers to form propagating quasi-dry modes (as in Fig. 3b). The half that decay at rate ϵ_c for all wavenumbers are associated with the q equations in the troposphere above the boundary layer. This was

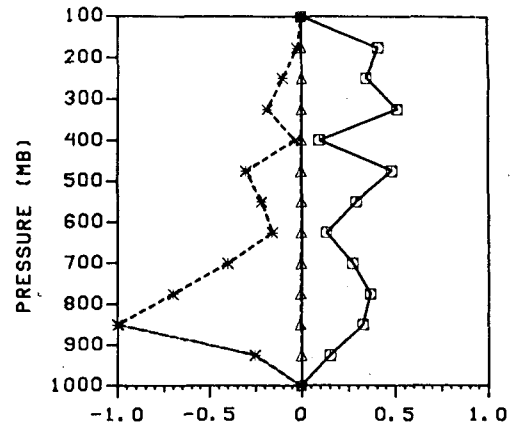

FIG. 4. An example of the energy and moisture budgets of the kinematically dominated modes ($\lambda \approx -\epsilon_m$) at wavenumber one. Solid line denotes time rate of change of temperature, circled solid line denotes latent heating, squared solid line denotes adiabatic cooling, triangled dashed line denotes time rate of change of moisture, starred dashed line denotes moisture sink, and crossed dashed line denotes moisture convergence. Note that the signs are arranged such that when adiabatic cooling exactly cancels latent heating, the two curves overlap; and similarly for moisture sink and moisture convergence.

confirmed by a distorted physics experiment in which artificial multipliers were placed in front of the time derivatives of these q equations. It is to these modes that the name "moisture modes" best applies. However, on the basis of the eigenstructures and dominant balances, it is nearly impossible to distinguish these from the other moisture-dominated modes at low wavenumbers, so we apply the same term to both.

Examining the energy and moisture budgets of the moisture modes (not shown), it is found that the moisture structures are wiggly in the vertical and that the thermodynamic components are negligible compared to the moisture variations. The dominant balance is between moisture sink and time rate of change of moisture. These properties were predicted by the analytical approach for modes of $\lambda = -\epsilon_c$. These modes bring perturbations of q quickly toward a quasi-adjusted state for all horizontal structures. Since these modes decay fast and at the same rate, they would not be seen individually during numerical time integration. Their individual eigenstructures are thus of little interest except to note that they are dominated by q components, and that these have successively higher numbers of zero crossings in the vertical.

c. Quasi-dry modes

In Fig. 3a, half of the moisture modes tend to merge with the kinematically dominated modes to become propagating waves with near-constant decay time of about $2\tau_c$ in the smaller-scale regime. These propagating modes have qualitatively similar dynamics to the internal modes in the dry atmosphere, with little involvement of moist processes; hence we refer them as

the "quasi-dry modes." The merging tendency and their properties can be better understood with a simple paradigm to interpret the scale-dependent growth rates of these modes. Combining equations (2.6) and (2.1b), for the Kelvin meridional case, yields a single vertical structure equation in the troposphere, that is,

$$\partial_p^2\omega' + m^2\omega' = \epsilon_c \frac{m^2}{\partial_p \bar{S}} C_p(T_c' - \Delta T_c')(q_b', T_b', \hat{T}', \hat{q}'), \quad (4.1)$$

where

$$m = \left[\frac{\kappa(\partial_p \bar{S}/p)}{(\lambda + \epsilon_m)(\lambda + \epsilon_r + \epsilon_c)}\right]^{1/2} k$$

is a complex variable with the real part denoting the vertical wavenumber, which is determined by the stratification of troposphere and eigenvalue for a given horizontal wavenumber k. Vertically averaged quantities are denoted by carets. Since the thermodynamics of the kinematically dominated modes are degenerate at leading order, the order τ_c thermodynamic variables enter the zeroth order ω in (4.1), keeping infinite degrees of freedom in the vertical (since $T_c^{(1)}$ is free). Since these modes are not very sensitive to the boundary-layer dynamics, their characteristic time scales are controlled mainly by the lhs of (4.1), that is, the stratification. When dry stratification comes to dominate over moist processes, the dispersion relation of the quasi-dry modes can be expressed as

$$(\lambda + \epsilon_m)(\lambda + \epsilon_r + \epsilon_c) + c_n^2 k^2 = 0, \quad (4.2)$$

where c_n is the effective atmospheric internal gravity wave phase speed determined by the atmospheric stratification. Equation (4.2) contains two roots of λ; that is,

$$\lambda = -\frac{(\epsilon_m + \epsilon_r + \epsilon_c)}{2} \pm \frac{1}{2}[(\epsilon_m - \epsilon_r - \epsilon_c)^2 - 4c_n^2k^2]^{1/2}. \quad (4.3)$$

For high wavenumbers ($c_nk \gg \epsilon_c$), (4.3) can be approximated as

$$\lambda \approx -\frac{(\epsilon_c + \epsilon_r + \epsilon_m)}{2} \pm ic_nk. \quad (4.4)$$

Thus, the quasi-dry modes propagate nondispersively with a near-constant decay rate of about twice of the convective time (since $\epsilon_c \gg \epsilon_m, \epsilon_r$).

For low wavenumbers, quasi-dry dynamics does not apply very well but, considering small k in (4.3), gives insight into the transition. For ($c_nk \ll \epsilon_c$), (4.3) becomes

$$\lambda \approx \begin{cases} -(\epsilon_c + \epsilon_r) \\ -\epsilon_m. \end{cases} \quad (4.5)$$

It is noted that only pure decay roots are permitted for planetary-scale waves. Since $\epsilon_c \gg \epsilon_r$, one root decays fast, at the time scale of cumulus convection, and the other root decays slowly, at the time scale of large-scale momentum damping. This explains the tendency of the quasi-dry modes to split into purely decaying modes with well-separated decay rates at low wavenumbers. The modes of decay rate ϵ_m correspond to the kinematically dominated modes (in fact, this paradigm also predicts the dominance of kinematic variables for these); the modes of decay rate $\sim \epsilon_c$ correspond to the moisture modes (for which this paradigm provides only an indication of the transition). With larger c_n, it is easier to satisfy the condition $c_nk \gg \epsilon_c$; thus, the transition occurs at smaller k. This property can be clearly seen in Fig. 3b: larger c_n (larger slope) modes tend to merge earlier at smaller k than those of smaller c_n (smaller slope).

As is well known, the existence of discrete, vertically trapped modes in the dry case is associated with the use of a rigid-lid condition; with a radiation condition this is replaced by a continuum of vertically radiating modes. Since GCMs cannot avoid having a top somewhere in the tropopause or stratosphere, these spurious modes will inevitably be generated during numerical integration. These results presented here suggest that under MCA, these modes will have minimal effect in deep convection regions due to their fast decay rates.

d. Stationary deep-convective mode

In Fig. 3a, we also find a stationary mode with slow decay rate even at high wavenumbers. This stationary mode has well-defined structures only at relatively large wavenumbers and merges into the slowly decaying, kinematically dominated modes at low wavenumbers. Figure 5 shows the energy and moisture budgets of this mode at wavenumber 25, which is roughly located at the scale of a typical GCM's grid size. This mode has a deep-convective structure with balances between latent heating (moisture source) and adiabatic cooling (moisture convergence). Since it decays slowly even at very high wavenumbers, it could potentially be unstable in a nonlinear, spatially inhomogeneous system. We thus suspect that this mode could be a candidate for the "gridpoint storms," which appeared in the GFDL GCM model. Although a detailed analysis of this mode is not presented here, these results indicate that all of the geophysically interesting properties of MCA in the smaller-scale regime will be associated with this mode.

5. Propagating deep-convective mode (Madden–Julian mode)

a. Stability, structures, and scale selectivity

A single vertical mode with complex eigenvalue is found among the slow modes in the planetary-scale regime. At wavenumber one, the eigenvalue gives a de-

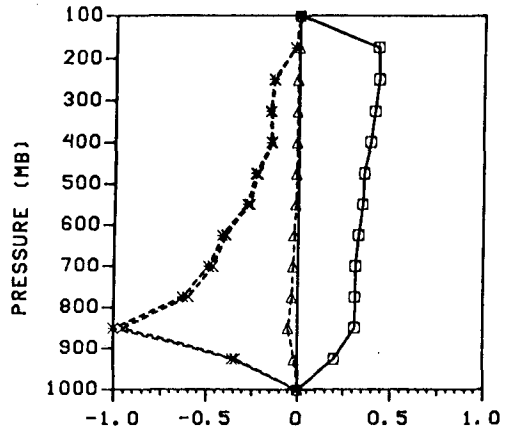

FIG. 5. As in Fig. 4 except for the stationary deep-convective mode at wavenumber 25.

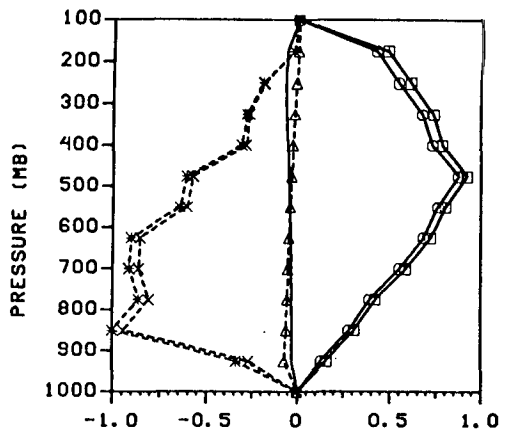

FIG. 6. As in Fig. 4 except for the Madden–Julian mode (i.e., the propagating deep-convective mode for Kelvin meridional structure).

cay time of about 10.8 days and a period of about 33.8 days for $\tau_c = 2$ hours. When momentum damping is removed, keeping thermal damping, the decay time decreases to 18 days. When both momentum and thermal dampings are removed, the decay time dramatically decreases to 180 days, close to neutral, as in the small τ_c case of NY. The phase speed, $c_r = 14$ m s^{-1}, would yield an equivalent depth c_r^2/g of about 20 m, although this is of limited value in interpreting this CID mode.

Figure 6 shows the energy and moisture budgets of this low-frequency mode. The balances are mainly between latent heating (moisture source) and adiabatic cooling (moisture convergence), while the time rate of change of temperature (moisture) is just a small residual of these two large terms. The maximum heating is at 500 mb, which is higher than the maximum moisture sink, suggesting strong vertical redistribution of moist static energy by the convective adjustment. The vertical structures of this propagating deep-convective mode along with its intraseasonal period at wavenumber one resemble the MJO observed in many GCMs or observations. It should be underlined that these profiles are determined internally by the convective interaction with dynamics—nothing in the convective scheme directly specifies the vertical heating distribution. We also note that this deep-convective structure remains unchanged and distinguishable to wavenumber 20.

Figure 7 shows the slow-mode eigenvalues as a function of wavenumber. The propagating deep-convective mode, which is embedded in the slow mode branch, is the only propagating mode; the rest of the modes are purely decaying kinematically dominated modes. The frequency curve shows that the propagating deep-convective mode is nearly nondispersive until wavenumber 10; this property is also found in a GCM study (Neelin et al. 1987). The propagating deep-convective mode is the least rapidly decaying at wavenumber one, but shows strong scale selectivity. While it is damped weakly by dissipation terms at wavenumber one, it is increasingly damped at higher wavenumbers due to the effect of finite τ_c. Those of the kinematically dominated modes that exhibit less strong scale selectivity than the propagating deep-convective mode have more complex vertical structures and would be damped by vertical diffusion if it were included. The scale selectivity by finite τ_c may be roughly understood in terms of the transition toward quasi-dry dynamics at high wavenumber. When k is small enough that τ_c is truly fast compared to time scales of dry dynamics, the thermodynamics closely obey convective adjustment constraints. However, as dry-dynamical balances begin to become important as k increases, the temperature structure no longer perfectly obeys these constraints and the convective adjustment acts as a damping effect on the imperfectly adjusted thermodynamics. At the low wavenumbers shown in Fig. 7,

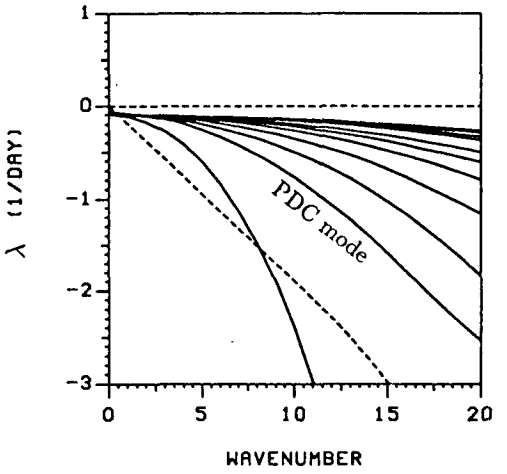

FIG. 7. Eigenvalues of slow modes as a function of wavenumber. Solid lines denote growth rates, with the curve for the propagating deep-convective (PDC) mode labeled. Dashed lines denote the frequency, but only the PDC mode has nonzero frequency. The wavenumber axis is labeled for the case of Kelvin meridional structure. The long Rossby wave case is obtained by rescaling wavenumber by $(2n + 1)$.

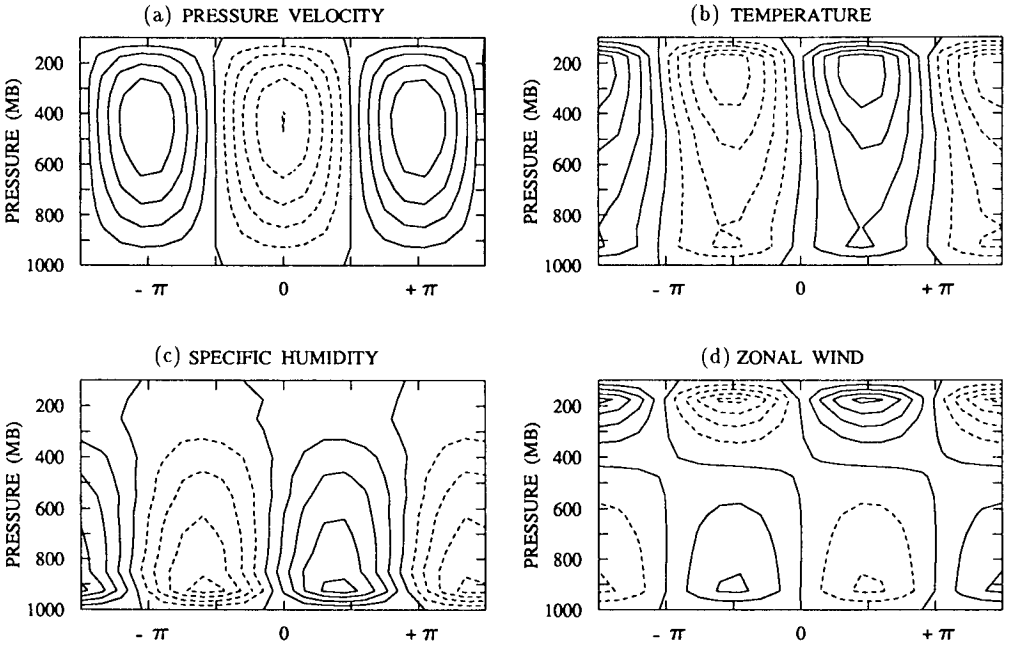

FIG. 8. Zonal cross section of the wavenumber one propagating deep-convective mode with Kelvin wave meridional structure (MJ mode) in (a) pressure velocity, (b) temperature, (c) specific humidity, and (d) zonal wind. Zonal phase is given in radians, since extremely similar structures occur for other low wavenumbers.

the convective adjustment constraints are obeyed quite closely so that damping rates are only a small fraction of τ_c^{-1}. However, since τ_c is small, this still provides significant scale selectivity.

To indicate the phase relation among physical quantities, Fig. 8 shows the eigenstructures of pressure velocity, temperature, specific humidity, and zonal wind on the zonal plane. It is found that the temperature and the moisture are in phase but trail pressure velocity by $\pi/2$. The pressure velocity has maximum at about 400 mb, consistent with observations in deep-convection regions (Yanai et al. 1973). The temperature has a maximum at about 300 mb along with a local maximum at the top of the PBL. However, the back tilt of the temperature in the upper troposphere and stratosphere found in the GFDL GCM simulations (Lau et al. 1988) is not present in our model due to the lack of a stratosphere. We also note that even though we do not include boundary-layer friction effects, the zonal wind in the upper troposphere is relatively stronger than in the lower troposphere, qualitatively similar to Lau et al. (1988).

b. *Sensitivity tests*

The sensitivity of the MJ mode to model parameters and basic-state quantities is tested here, noting that changes in the convective parameters are applied only to the perturbation dynamics, with the basic state kept constant. Figure 9a shows the eigenvalue of the wavenumber one propagating deep-convective mode (MJ mode) as a function of τ_c. The MJ mode decays monotonically with increasing τ_c, but the frequency of the MJ mode appears not to be very sensitive to the value of τ_c. Because the finite τ_c effects tend to stabilize the MJ mode, we expect this mode to be more stable with larger τ_c. In the fast-adjustment limit ($\tau_c \to 0$), the analytical approach derived in NY becomes the exact solution. For $\tau_c = 30$ minutes, the numerical result (not shown) is very close to the analytical approach.

Figure 9b shows the eigenvalue of the MJ mode as a function of basic-state boundary-layer moisture, $\bar{q}_b$. We note that varying $\bar{q}_b$ in isolation is a simplification of processes that might affect the basic state. The tropospheric temperature of the basic state in general changes with $\bar{q}_b$, but as long as $\bar{S}$ changes by a constant value in p, the stratification is unaffected. The variation of $\bar{q}_b$ thus provides a good case to illustrate a numerical effect due to the discretization of cloud top. For the vertical resolution used here ($\Delta p = 75$ mb), the layer within which cloud top occurs does not change for $\bar{q}_b$ in the range shown (17 to 21 g kg^{-1}). The growth rate is not sensitive to $\bar{q}_b$ change, but the frequency of the MJ mode decreases significantly with increasing $\bar{q}_b$: the period increases to 48 days at $\bar{q}_b = 21$ g kg^{-1} compared to a period of 33.5 days at $\bar{q}_b = 18$ g kg^{-1}. Aside from feedback mechanisms, both features are consistent with the analytical theory in that only the damping effects can affect the growth rate, while the period of the MJ mode is dictated by the "gross moist stability," ΔM. When the atmosphere contains more moisture in the boundary layer, for fixed cloud top, the atmosphere tends to be less stable (hence smaller ΔM) and the period of MJ mode becomes longer. The sensitivity of the period has potential implications for GCMs that

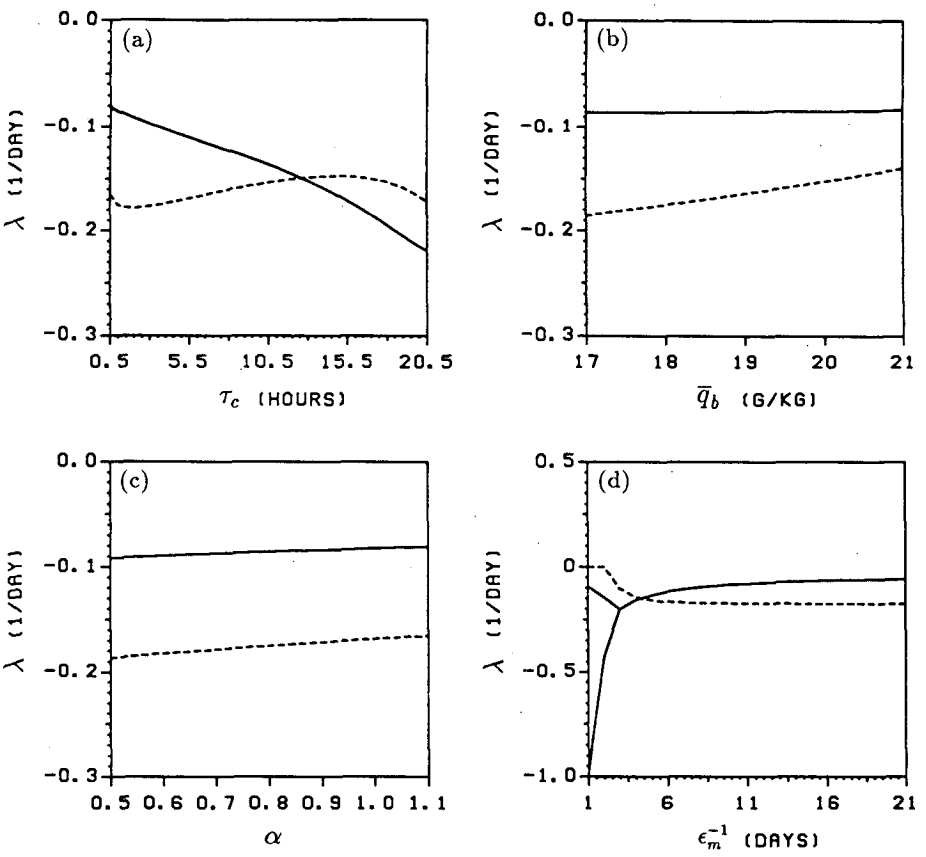

FIG. 9. (a) Eigenvalue of MJ mode as a function of the cumulus adjustment time, τ_c, with solid line denoting growth rate and dashed line denoting frequency. (b) As in (a) except as a function of the basic-state PBL specific humidity, $\bar{q}_b$. (c) As in (a) except as a function of the subsaturation parameter, α. (d) As in (a) except as a function of the Rayleigh damping time, ϵ_m^{-1}.

have similar vertical resolution and hence similar discretization of cloud top. Under standard differencing, such as is used here, this gives a *systematic error* because the effective numerical cloud top is at the top of the layer within which true cloud top would occur. Thus, this will yield a numerical phase speed that is always greater than it should be.

Figure 9c shows the eigenvalue of the MJ mode as a function of the subsaturation parameter, α. Neither growth rate nor frequency is sensitive to the change of α, even allowing a large range of variation, from substantial subsaturation to supersaturation. Figure 9d shows the eigenvalue of the MJ mode as a function of the inverse Rayleigh friction rate, ϵ_m^{-1}. We find that when ϵ_m is in the reasonable range, the MJ mode is oscillatory with almost constant period independent of ϵ_m. The Rayleigh damping time scale has to be unrealistically strong, less than 2 days through the whole troposphere, for the frictional effect to break the oscillation tendency.

c. *Evaporation–wind feedback*

The evaporation–wind feedback, formulated in NY, is included in this subsection for the Kelvin wave case. The evaporation–wind feedback for the Rossby wave case is slightly more complex to analyze and tends to merely have a damping effect. The effective evaporative damping effect is kept, with a value of (2 days)$^{-1}$ for ϵ_q. Figure 10 shows the growth rate as a function of the evaporation–wind feedback parameter, F, for the MJ mode at wavenumber one. We note that the magnitude of the evaporation–wind feedback constant, $F \equiv -\text{sgn}(\bar{u}_b)\rho C_D[\bar{q}_{\text{sat}}(T_s) - \bar{q}_b]$, is proportional to the basic-state water vapor mixing ratio difference between sea surface level, $\bar{q}_{\text{sat}}(T_s)$, and the boundary layer, $\bar{q}_b$, as well as the drag coefficient, C_D. It is found that the eastward propagating MJ mode is destabilized when the evaporation–wind feedback is included (the anti-Kelvin wave is included only as an example of the effects on westward propagating waves). With $F > 0.13$ mm day^{-1} (m s^{-1})$^{-1}$, the eastward moving MJ mode becomes unstable. We note that this is the only vertical mode destabilized by the evaporation–wind feedback. The frequency of the MJ mode increases only slightly with F. Figure 11 shows the growth rate of the propagating deep-convective mode as a function of wavenumber for different values of the evaporation–

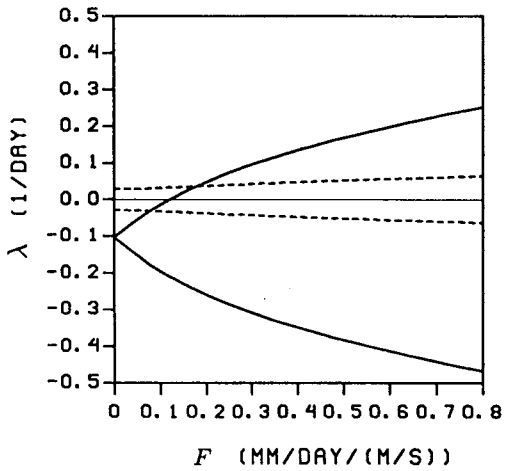

FIG. 10. Eigenvalue of MJ mode as a function of the evaporation–wind feedback parameter, F [in units of mm day^{-1} (m s^{-1})$^{-1}$]. Solid line denotes growth rate and dashed line denotes frequency.

wind feedback parameter, F. At $F = 0.2$ mm day^{-1} (m s^{-1})$^{-1}$, wavenumber one is the most unstable wave with an e-folding time of about 20 days; while at $F = 0.4$ mm day^{-1} (m s^{-1})$^{-1}$, wavenumber two becomes the most unstable wave with an e-folding time of about 6 days.

From the above results, we are led to conclude that traditional ideas about wave–CISK in interpreting the large-scale perturbations resulting from interaction between large-scale dynamics and the cumulus convection should be modified regarding stability aspects. CISK, in the sense of instability, does not exist for the very reasonable convective scheme investigated here, and it is unlikely to be responsible for exciting the large-scale equatorial perturbations. However, convective interaction with dynamics (CID) does single out one vertical mode, which for the Kelvin wave case corresponds well in vertical structure and phase speed to the MJO. The MJ mode can be destabilized by the evaporation–wind feedback, and the scale selectivity favoring the MJO at planetary scales can arise from the effects of finite cumulus adjustment time, which tends to damp the short-scale waves.

6. Stochastic forcing

To understand the bulk effect of stochastic forcing on the power spectrum of the tropical troposphere, the forced version of (2.15) is employed. The stochastic forcing can be justified as random forcing resulting from nonresolved, "mesoscale" processes occurring at scales smaller than the Reynolds average of the convective parameterization, in comparison to observations; or from poorly resolved grid-scale processes, in comparison to GCMs. We consider a forcing that is random in x and t but has a specified vertical structure (which can be different in the momentum equations and in the thermodynamic equations) and Kelvin wave meridional structure. Similar results will hold for other meridional modes. Fourier decomposing in basis functions $\exp[i(kx - \sigma t)]$, where σ and k are the frequency and wavenumber of the tropical variance, with $\sigma k > 0$ appropriate to the Kelvin wave, the forced problem has the form:

$$(\mathbf{A} - i\sigma\mathbf{B})\tilde{\mathbf{X}} = \tilde{F}(\sigma, k)\mathbf{f}, \tag{6.1}$$

where $\tilde{\mathbf{X}}$ denotes the Fourier-transformed response vector of ω, T, and q at each level for a given frequency and wavenumber, $\tilde{F}(\sigma, k)$ represents the Fourier-transformed x–t structure of the forcing, and $\mathbf{f}$ denotes the vertical structure including both thermodynamical and kinematical sources. For fixed vertical structure and fixed partition between kinematic and thermodynamic forcing, we can write

$$\tilde{\mathbf{X}} = \mathbf{H}(\sigma, k)\tilde{F}(\sigma, k), \tag{6.2}$$

where

$$H_j = (\mathbf{A} - i\sigma\mathbf{B})^{-1} f_j \tag{6.3}$$

is the transfer function for a given variable and level (the index j running through levels for ω, T, q). As for any stable, linear, time-invariant filter, the power spectral density of the response, $S_{\tilde{X}_j}$, to random forcing of input spectral density, $S_{\tilde{F}}$ is just

$$S_{\tilde{X}_j} = |H_j|^2 S_{\tilde{F}}, \tag{6.4}$$

where we note that the atmospheric "filter" is stable in absence of evaporation–wind feedback. Here, a white-noise distribution of the forcing in both frequency and wavenumber domains is employed for two reasons: (i) it provides an estimate of the extent to which the large-scale moist dynamics can select a specific scale and frequency of the perturbations resulting from sub-Reynolds-scale stochastic forcing; (ii) the stochastic forcing is considered to arise from processes that are small scale in terms of spatial and temporal correlation, so it is very reasonable to model their expression at low wavenumbers and frequencies as white.

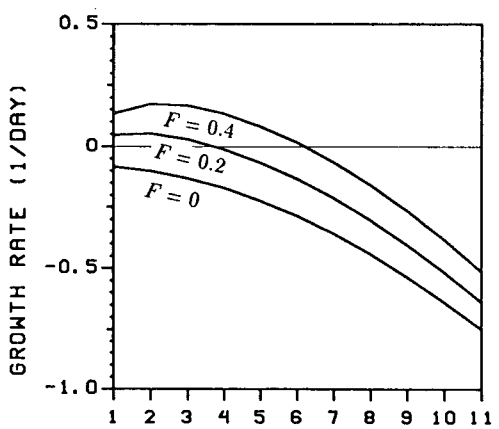

FIG. 11. Growth rate of MJ mode as a function of wavenumber for different value of F.

The power spectral densities of the response are calculated at each level for representative forcing structures. For ease of display, Figs. 12 and 13 show the average over all levels of the power spectral density of T, u, ω and precipitation, P, in wavenumber–frequency domain for the Kelvin wave. Figure 12 shows the case of a purely thermodynamic forcing in the boundary-layer temperature equation, while Fig. 13 shows the case of a purely kinematic forcing in the boundary-layer ω equation. Amplitudes of the power spectral density of the forcing are not well known for the subgrid-scale processes. For thermodynamic forcing we have no direct estimates so we use 4 $(\text{K day}^{-1})^2$ day, which is chosen so that the flatter parts of the P spectrum roughly match an estimate of the "white" background in P from GFDL GCM grid-scale processes from Lau et al. (1988). For kinematic forcing, we attempt a rough estimate of grid-scale noise forcing as follows: from Hayashi (1974), the GFDL GCM has a "white" background power spectral density of around 300 $(\text{mb day}^{-1})^2$ day at 825 mb. We assume PBL forcing to create similar velocities near the top of the PBL with zero velocity at the surface, leading to forcing in the omega equation of around 1×10^{-5} [(mb day^{-1})/(mb^2 day)]^2 day. Different estimates would simply rescale the figures.

In Fig. 12, the maximum power spectral densities at planetary scales occur at a nearly constant phase speed of about 14 m s^{-1}, corresponding to a period of about 35 days at wavenumber one. Along with the vertical structures (not shown), both indicate dominance of the propagating deep-convective mode discussed in section 5. The temperature component (Fig. 12a) shows significant spectral densities in the planetary-scale, low-frequency domain with a maximum amplitude near 0.6 K^2 day; the zonal wind component (Fig. 12b) also indicates dominance of spectral densities in the planetary scale with a local maximum just over 4 $(\text{m s}^{-1})^2$ day at wavenumber one, both suggesting strong planetary-scale selection in exciting the low-frequency MJ mode by the thermal stochastic forcing. We also note that pressure–velocity spectral densities are larger at higher frequency and shorter wavelength (Fig. 12c), compared to zonal wind spectral densities, which in turn emphasize higher frequency and wavenumber than T, as one would expect from wave dynamics. However, the scale selectivity is not strong enough to keep the spectral density maximum of ω at the lowest wavenumbers. The precipitation (Fig. 12d) exhibits a spectral density distribution similar to that of the pressure velocity with a maximum power spectral density just over 40 $(\text{mm day}^{-1})^2$ day, near wavenumber four or five. This is consistent with the

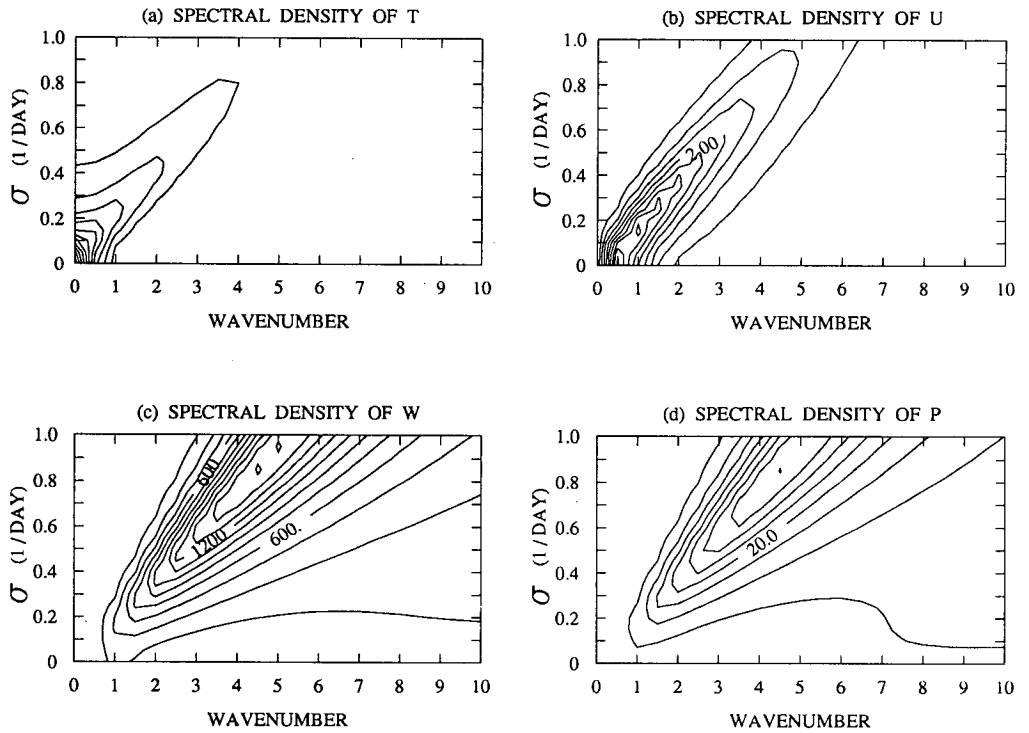

FIG. 12. Average over all vertical levels of the power spectral density in the frequency–wavenumber domain of the Kelvin wave case in the tropical troposphere resulting from spatially and temporally white, thermal stochastic forcing. A forcing rate of 4 $(\text{K day}^{-1})^2$ day is used in the boundary-layer thermodynamic equation. (a) Power spectral density of the temperature, with contour interval of 0.05 K^2 day, (b) power spectral density of the zonal wind, with contour interval of 0.5 $(\text{m s}^{-1})^2$ day, (c) power spectral density of the pressure velocity, with contour interval of 150 $(\text{mb day}^{-1})^2$ day, and (d) power spectral density of the precipitation, with contour interval of 5 $(\text{mm day}^{-1})^2$ day.

GCM peaks of Lau et al. (1988) except that the GCM maximum occurs at wavenumber two or three. Moisture spectra (not shown) resemble T spectra in all respects.

In the kinematically forced case (Fig. 13), we find that strong planetary-scale selectivity is also observed. However, the power spectral density distribution is dominated by stationary waves at planetary scales due to the excitation of kinematically dominated modes, with only a weak response of the propagating waves. Because the propagating deep-convective mode is less strongly excited by the kinematical forcing, the maximum pressure–velocity response appears at very low-frequency and planetary scales. The vertical structures of these stationary modes (not shown) also strongly indicate dominance of the slowly decaying, kinematically dominated modes. The amplitudes of pressure–velocity and precipitation are considerably weaker than the GCM spectra (Hayashi 1974; Lau et al. 1988), but this could simply be due to our estimate of the forcing spectral density.

7. Conclusions

Strong interaction between cumulus-scale convection and the large-scale circulation is crucial to the dynamics of tropical climate variability. In these two papers, we examine this interaction in the context of a moist convective adjustment (MCA) cumulus parameterization scheme. In particular, the Betts–Miller scheme (Betts 1986; Betts and Miller 1986) is used, which is smoother than classical MCA (Manabe 1965) due to the introduction of a relaxation time in adjusting toward the reference state. With the MCA parameterization, the net effect of the ensemble of convective motions at scales below the Reynolds average in space and time (sub-Reynolds scales or subgrid scales) is parameterized such that the large scale and sub-Reynolds scales are strongly linked through thermodynamic constraints (type I closure; Arakawa and Chen 1987). The vertical form of the thermodynamic reference profiles are determined by $\gamma = d(Lq_{sat})/d(C_pT)$. However, the modes of the large-scale circulation under MCA have dynamical structures, including heating and moistening profiles, that are determined by convective interaction with dynamics (CID) rather than simply by γ. We introduced the term CID in NY to distinguish convective interaction with dynamics in general from the more specific term CISK (conditional instability of the second kind), which presumes that the large-scale flow can actually become unstable through its interaction with the net effects of sub-Reynolds-scale convection. CISK thus implies an assumption that the large-scale circulation can access column instability—as measured, for example, by the conventional parcel-based quantity CAPE (convective available potential energy) or the column-based MAE (moist available energy; Randall and Wang 1992).

As in Part I, we break our conclusions down into a summary of specific results regarding how a smooth

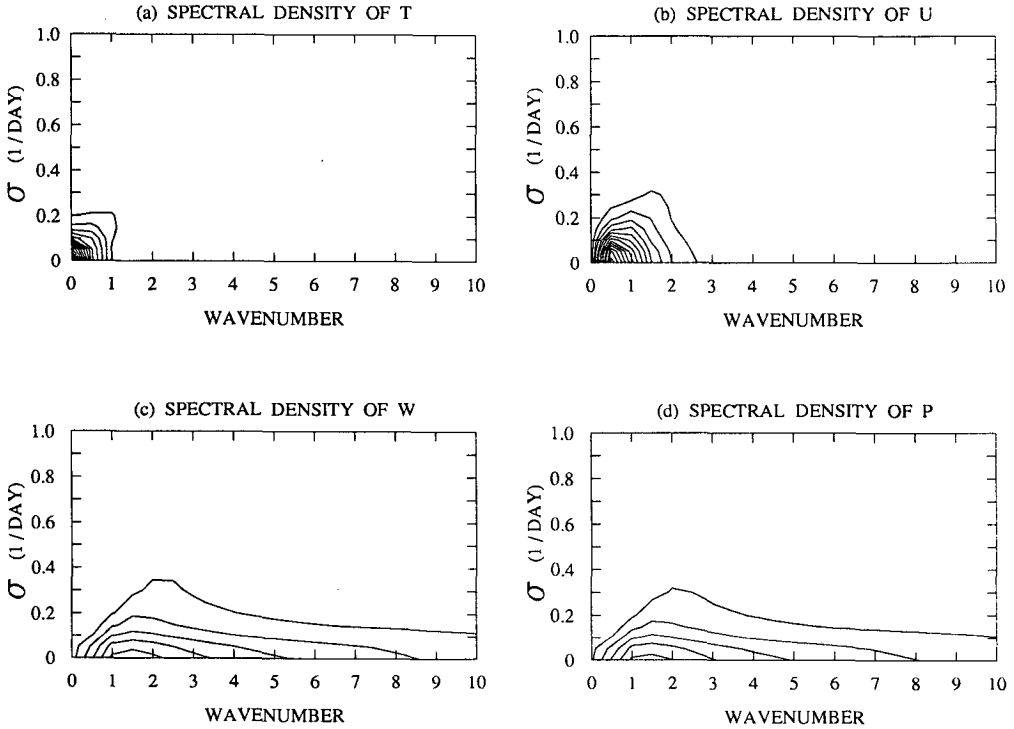

FIG. 13. As in Fig. 12 except for white, kinematical stochastic forcing applied in the ω-equation with a forcing rate of 300 (mb day^{-1})^2 day.

MCA scheme behaves and how geophysical phenomena, especially the MJO, arise under MCA—and a more general discussion of implications for a possible view of the tropical atmosphere.

a. Summary

In NY, we examined the CID modes of the time-dependent problem analytically, in the limit where cumulus adjustment time, τ_c, is small compared to the time scales of large-scale dynamics, an assumption which holds best at low wavenumbers. We reexamine the model numerically in Part II, concentrating on the Kelvin meridional mode case for which the simplest form of the vertical structure equations is valid uniformly for all zonal wavenumbers. We emphasize that the *same results apply to long Rossby waves and short gravity waves,* as discussed in section 2. The numerical results at planetary scales are consistent with the analytical approach. The eigenmodes at large scales are well separated into two stable regimes. The fast modes adjust quickly toward the reference atmosphere at the convective time scale, while the slow modes evolve at the time scale set by the large-scale dynamics. All modes are stable for all wavenumbers. The finite τ_c effect tends to further stabilize all the slow modes relative to the analytical calculations. Thus, "CISK," in the sense of instability, does not occur for this convective scheme, at least not for the separable case in a homogeneous basic state. Kelvin wave CID singles out one vertical mode with slow phase speed and deep-convective structure resembling the MJO at planetary scale. In addition to confirming analytical results, the numerical approach provides the following additional insights:

1) The MCA scheme exhibits a property that almost all the high wavenumber waves are internally decaying much more quickly than the low wavenumber waves, giving strong scale selectivity. This is in striking contrast to CISK studies using Kuo-like schemes for which linear instability tends to be large at smaller scales. The scale selectivity is sensitive to the magnitude of the convective adjustment time scale, τ_c. With larger τ_c (such as would occur in a case where the atmosphere is not deep convective everywhere or taking into account a longer effective adjustment time in presence of sub-Reynolds-scale mesoscale organization), even stronger scale selectivity in favor of planetary scales occurs.

2) The analytical approach in Part I accounts only for modes at planetary scale where the characteristic time scale of the dynamics is much longer than τ_c. The structures and behavior of eigenmodes are most easily understood from the numerical calculations. The eigenmodes can be subdivided into classes according to dynamical behavior and the dominant variables in the eigenvectors. For instance, "moisture modes" have structures dominated by the moisture components. Half of the moisture modes tend to merge with the kinematically dominated modes at higher wavenumbers to become propagating "quasi-dry modes;" the other half have fast decay rates around ϵ_c for all wavenumbers. The latter tend to bring moisture perturbations quickly back to an adjusted state for all horizontal wavenumbers and almost all vertical structures (except that of the propagating deep-convective mode). However, they would not be seen individually in time integrations since they decay rapidly and all at the same rate. The remainder of the eigenmodes are most easily classified within two separate spatial scale regimes, based on the finite τ_c effect in the wavenumber domain: the "planetary regime," in which τ_c is indeed small relative to dynamical time scales; and the "smaller-scale regime," in which τ_c cannot be regarded as small. In the planetary regime, the classification is similar to that described in NY: in the class of "slow modes," there is a single geophysically important "propagating deep-convective mode" and a less important set of stationary modes dominated by kinematic variables with small thermodynamic components.

3) In the smaller-scale regime, the kinematically dominated modes, along with half of the moisture modes, individually become propagating and asymptote to a constant decay time of about $2\tau_c$ at large wavenumbers. This behavior roughly follows a simple damped gravity wave paradigm, with cumulus heating acting almost entirely like a strong damping, since the dynamics of these modes tends to be nearly decoupled from the boundary-layer thermodynamics. Like all vertically trapped internal modes in tropical models, these quasi-dry modes are spurious modes in the sense that they depend on the use of a rigid-lid condition. If a radiation upper boundary condition were used, these would radiate upward. The fact that MCA causes these to decay rapidly at small scales in convective regions is thus numerically desirable. We also find a "stationary deep-convective mode" at a broad range of wavenumbers for which τ_c is not small. Its behavior is distinctive, with slow decay rate even at high wavenumbers, and it exhibits deep-convective structure even to very small scales. This mode is a possible candidate for the "gridpoint storms" that appear in the GFDL GCM, which uses a classical MCA parameterization. Since the stationary deep-convective mode is close to neutral at high wavenumbers in our analysis, it could plausibly be destabilized by spatial inhomogeneities or by discontinuous convection criteria in a numerical model.

4) The propagating deep-convective mode has scale selectivity in favor of planetary-scale waves due to the finite τ_c effect under the CID mechanism alone, even with a rigid-lid condition. For the wavenumber one Kelvin wave meridional structure, it has a period of about 33 days, which, along with its vertical structure, is highly suggestive of the observed tropical Madden–Julian Oscillation. In Part I we noted that use of a radiation vertical boundary condition could significantly slow its phase speed; here we note that vertical discretization results in phase speeds that are systematically too fast. Both may have implications for the fast phase speeds found in many GCMs. When the evapo-

ration–wind feedback mechanism is included, wavenumber one or two is selectively destabilized with growth rate on the order of about (10 days)$^{-1}$ for a reasonable range of the evaporation–wind feedback parameters. The frequency dependence on wavenumber is almost nondispersive.

5) Although the evaporation–wind feedback provides a plausible mechanism for the MJO involving instability, it is also necessary to consider that the MJO may be a slowly decaying mode excited by external forcing. We consider two possible sources of forcing: lateral forcing from midlatitudes and tropical stochastic forcing by nonresolved mesoscale processes. The possibility of lateral forcing of tropical large-scale waves has been raised by many authors (Yanai and Lu 1983; Itoh and Gill 1988; Hsu et al. 1990; Zhang and Webster 1992; Zhang 1992). This is potentially a complex process—we provide a preliminary examination of the simplest case (see appendix), in which a lateral mobile forcing is applied in a background state with barotropic mean zonal wind. The results suggest that such effects are very modest in the simple situation examined here. If they are to be important, it must be through more complicated processes (such as zonal inhomogeneity in the basic state or nonlinear interactions). On the other hand, stochastic forcing from nonresolved tropical processes does produce substantial variance at planetary scales for the "moist Kelvin wave" or the MJO. When the troposphere is forced thermodynamically by sub-Reynolds-scale white noise forcing (which we apply in the PBL), the propagating deep-convective mode is selectively excited, especially at planetary scales—although the scale selectivity in the case examined here is not as strong as observations or the GFDL GCM. However, when the troposphere is forced kinematically, the stationary, slowly decaying kinematically dominated modes account for the dominant variance of the tropical response. Similar results would apply for other meridional structures.

b. Discussion

Both the analytical results of Part I and the numerical results presented here indicate that there is no instability through CISK at large scales under MCA. This is in marked contrast to many CISK studies using simplified "Kuo-like" parameterizations. This difference between MCA and Kuo-like schemes may help shed light on the debate raised by Xu and Emanuel (1989) and Randall and Wang (1992) in observational studies, suggesting that there appears to be very little CAPE or MAE, respectively, available in the tropical atmosphere to support large-scale instabilities. The results implied by the closure assumptions of MCA are consistent with this: the column instability (as measured by MAE or CAPE) tends to be dissipated at the sub–Reynolds scales so the average amount remaining tends to be small. The debate about large-scale instability has so far focused on the question of just how small the MAE or CAPE is. Our results bring out a new aspect, namely, that under smoothly posed MCA, even if this amount is not very small, it is still not generally accessible as an energy source for the resolved, supra-Reynolds-scale motions. These motions evolve in a stable manner under quasi-equilibrium thermodynamic constraints imposed by the sub-Reynolds-scale convection as represented by MCA. Thus, under the assumptions of MCA, there can be nonzero CAPE and still no CISK.

If one leaves aside the selective instability of the MJO due to the evaporation–wind feedback, this stability of CID modes under MCA raises the question of how the power density spectrum of the tropical atmosphere is maintained. A self-consistent answer to this is provided by considering the effects on the large scales of stochastic forcing from the small scales. Cumulus parameterizations traditionally consider only the first-moment ensemble average of heating and moisture sink due to the sub–Reynolds scales. There are, of course, higher-moment effects (for instance, see Xu et al. 1992; Arakawa 1994), notably variance of the cumulus heating (and other forcing terms) about the ensemble mean that is parameterized in terms of the large-scale flow. This creates a random forcing on the large scales. The stochastic term can be reasonably treated as white in space and time at the large scales since the random process will have low spatial and temporal correlation between one Reynolds average domain and adjacent ones. Because of this, and because our model is stable (if the evaporation–wind feedback is not too large) and linearizable, it is straightforward to make quantitative statements regarding the form of the large-scale power spectral density, as a function of wavenumber and frequency, that can be driven by such sub–Reynolds noise. It has been pointed out to us by A. Arakawa that this may be one of the first attempts to examine explicitly the effects on large scales of the variance of cumulus heating about its parameterized value. Unfortunately, wavenumber–frequency power spectral density estimates of the appropriate dynamical quantities are not available for the observed tropical atmosphere, so we have compared instead to published results from the GFDL GCM. This requires interpreting the random process as arising from poorly resolved grid-scale processes, which is less clean than the argument for the case of the continuous atmosphere. Nonetheless, the results suggest that stochastic forcing (by processes that are small scale in the sense of spatial and temporal correlation) can indeed account for a substantial fraction of the large-scale variance, and that the selective wavenumber–frequency response of a stable CID model can provide a plausible, self-consistent explanation for the form of the power spectral density.

The implications for the Madden–Julian Oscillation are that Kelvin wave CID is responsible only for determining the overall structure of the MJO but that it is maintained by other mechanisms. In particular, instability due to the evaporation–wind feedback and ex-

citation by tropical stochastic forcing due to sub-Reynolds-scale thermal noise are both shown to be likely mechanisms. Scale selectivity favoring the MJO at planetary scales arises both from the effects of finite cumulus adjustment time, as shown here, and from upward radiation of shorter-scale waves, as shown in NY.

Acknowledgments. This work was supported in part by NSF Grant ATM-9215090 and NOAA Grant NA16RC0178 (the views expressed are those of the authors and do not necessarily reflect those of NOAA). One of the authors (JYY) was also supported in part by a postgraduate scholarship from the Ministry of Education, Republic of China. It is a pleasure to acknowledge discussions with A. Arakawa, A. Betts, C. Bretherton, K. Fraedrich, Y. Hayashi, I. Held, N.-C. Lau, S. Manabe, R. Lindzen, R. Seager, M. Suarez, and M. Yanai; we especially thank K. Emanuel for encouraging us to be explicit about the implications of our conclusions. Criticisms from an anonymous reviewer helped to strengthen our argument.

APPENDIX

Extratropical Mobile Forcing with Mean Zonal Flow

To provide a preliminary examination of the effects of midlatitude mobile forcing on the large-scale tropical waves, a linear, three-dimensional version of the model is examined in this appendix, with latitude-dependent barotropic zonal wind, $\bar{u}$, in the basic state. For perturbation solutions of the form $\exp[i(kx - \sigma t)]$, the complete set of equations are (2.1a–e) except that λ in all equations is replaced by $\lambda_T = (-i\sigma + ik\bar{u})$ and the Fourier transformed operator $\mathcal{L}_{\lambda,k,y}$ in (2.1f) is redefined as

$$\mathcal{L}_{\lambda_T,k,y} = \frac{(\lambda_T + \epsilon_m)}{(\lambda_T + \epsilon_m)^2 + \beta^2 y^2 - \beta y \partial_y \bar{u}} \partial_y^2 - \frac{(\lambda_T + \epsilon_m)\{2\beta^2 y + \partial_y \bar{u}[2ik(\lambda_T + \epsilon_m) - \beta] - \beta y \partial_y^2 \bar{u}\}}{[(\lambda_T + \epsilon_m)^2 + \beta^2 y^2 - \beta y \partial_y \bar{u}]^2} \partial_y$$
$$- \left\{ \frac{ik\beta + k^2(\lambda_T + \epsilon_m)}{(\lambda_T + \epsilon_m)^2 + \beta^2 y^2 - \beta y \partial_y \bar{u}} - \frac{2ik\beta^3 y^2 - \beta y \partial_y \bar{u}[2k^2(\lambda_T + \epsilon_m) + ik\beta] - ik\beta^2 y^2 \partial_y^2 \bar{u}}{[(\lambda_T + \epsilon_m)^2 + \beta^2 y^2 - \beta y \partial_y \bar{u}]^2} \right\}, \quad \text{(A.1)}$$

where σ and k are, respectively, the perturbation frequency and wavenumber determined by the forcing, and we have neglected the lower boundary pressure tendency due to the existence of mean zonal wind.

For this extratropically forced case, a semispectral version of the model is used: finite differenced in the vertical and meridional, and spectral in the zonal directions. For results shown here, 12 vertical levels and a 2-degree grid in latitude are used. Rather than forced from a lateral boundary (Itoh and Ghil 1988), we apply forcing within the domain but at off-equatorial latitudes. Walls ($v = 0$) at $\pm 40°$ latitude are used, but do not influence the tropical response. The matrix form of the problem gives

$$\mathbf{E}\tilde{\mathbf{X}} = \tilde{F}(k, \sigma)\mathbf{f}, \quad \text{(A.2)}$$

where $\mathbf{E}$ is a complex band matrix with most of the nonzero elements aligned along the diagonal and $\tilde{\mathbf{X}}$ is the Fourier-transformed solution vector containing $\tilde{\omega}$, $\tilde{T}$, and $\tilde{q}$. Here $\tilde{F}(\sigma, k)$ is the forcing vector due to either temperature tendency or pressure velocity anomalies of the travelling midlatitude system and $\mathbf{f}$ is again the vertical structure of the forcing.

The forcing and mean zonal wind structures are shown in Fig. A1. The maximum forcing represents 1 K day^{-1} heating rate in the thermodynamic equation. The forcing distribution roughly represents the shallow structure typical of midlatitude systems. Since we are interested in whether the MJO can be forced by planetary-scale midlatitude perturbations, consider an example of midlatitudinal wavenumber-one eastward

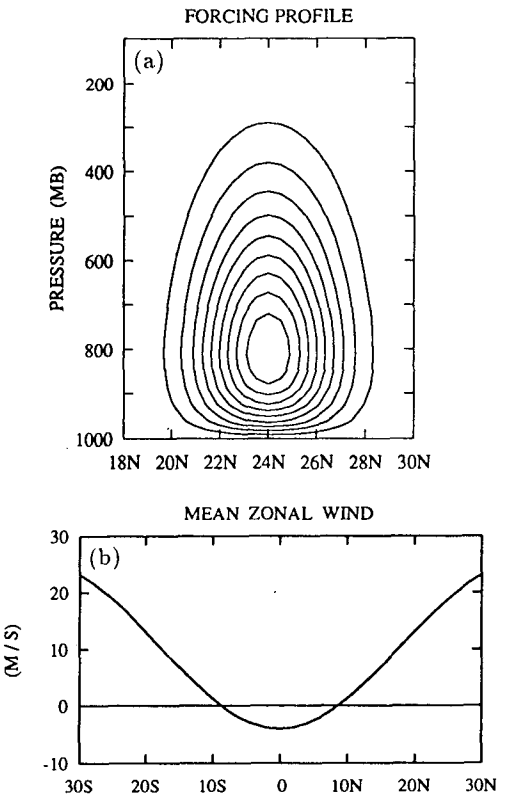

FIG. A1. (a) Distribution in the meridional–vertical plane of the extratropical diabatic forcing, with a maximum of 1 K/day. (b) Basic-state mean zonal wind profile.

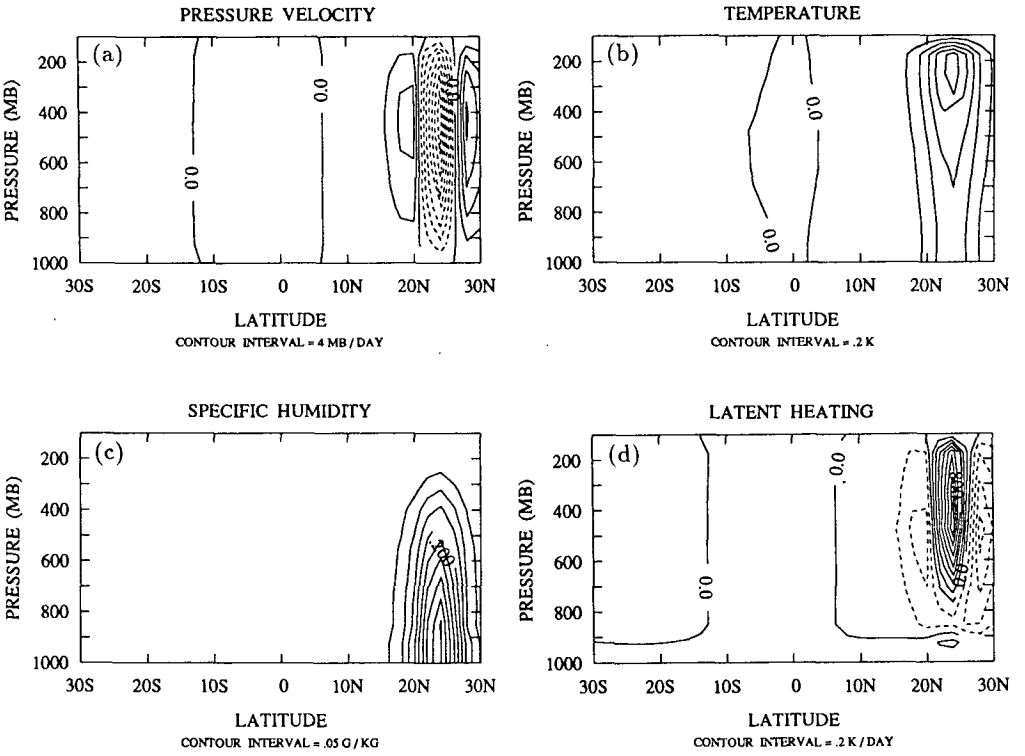

FIG. A2. The meridional cross section of the model response on the intraseasonal time scale of 60-day period. (a) Pressure velocity with contour interval of 4 mb/day. (b) Temperature with contour interval of 0.2 K. (c) Specific humidity with contour interval of 0.05 g kg^{-1}. (d) Latent heat response with contour interval of 0.2 K/day.

propagating temperature forcing with a period of 60 days, which would be expected to be favorable for forcing the MJO. Figure A2 shows the meridional cross section of the response. Strong local response is confined near the forcing region with deep structures resembling the propagating deep convective mode in the

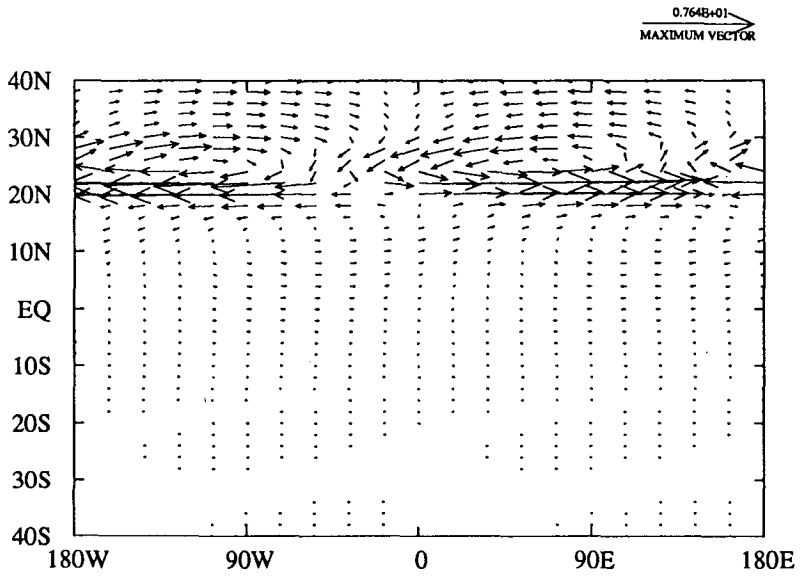

FIG. A3. The low-level wind (962.5 mb) response on the intraseasonal time scale of 60-day period. The maximum wind reaches 7.6 m s^{-1} near 20°N.

tropics. Only relatively weak response is found in the tropics or in the Southern Hemisphere. Figure A3 shows the low-level wind response at 962.5 mb. We note that the local response is not symmetric about the forcing center but has larger amplitude in the south than that in the north due to β effect [similar results can be found in Webster (1981) and Zhang (1992)]. For this damped, driven system, the critical line at around 18°N does not crucially affect the local response. However, the disturbance is unable to "tunnel through" the evanescent zone (equatorward the critical line) with sufficient amplitude to produce significant response in the equatorial waveguide. This result is not strongly sensitive to the phase speed of the forcing, nor to the zonal wavenumber, nor to kinematic rather than thermodynamic forcing.

The effects of midlatitude forcing, however, could be very different in a zonally inhomogeneous basic state (Webster and Holton 1982) or with precipitating/nonprecipitating regions in the basic state. Since treatment of these is beyond the scope of this paper, we by no means exclude possible excitation from midlatitudes. Rather, we simply point out that it must occur by processes more complex than the simplest case considered here.

REFERENCES

Arakawa, A., 1994: Closure assumptions in the cumulus parameterization problem. *The Representation of Cumulus Convection in Numerical Models of the Atmosphere,* K. A. Emanuel and D. J. Raymond, Eds., Amer. Meteor. Soc., in press.

——, and W. H. Schubert, 1974: Interaction of a cumulus cloud ensemble with the large-scale environment, Part I. *J. Atmos. Sci.,* **31,** 674–701.

——, and J. Chen, 1987: Closure assumptions in the cumulus parameterization problem. *Collection of Papers Presented at the WMO/IUGG Symp. on Short- and Medium-Range Numerical Weather Prediction,* Tokyo, 107–131.

Betts, A. K., 1986: A new convective adjustment scheme. Part I: Observational and theoretical basis. *Quart. J. Roy. Meteor. Soc.,* **112,** 677–691.

——, and M. J. Miller, 1986: A new convective adjustment scheme. Part II: Single column tests using GATE wave, BOMEX, ATEX and arctic air-mass data sets. *Quart. J. Roy. Meteor. Soc.,* **112,** 693–709.

Crum, F. X., and D. E. Stevens, 1983: A comparison of two cumulus parameterization schemes in a linear model of wave–CISK. *J. Atmos. Sci.,* **40,** 2671–2688.

Hayashi, Y., 1974: Spectral analysis of tropical disturbances appearing in a GFDL general circulation model. *J. Atmos. Sci.,* **31,** 180–218.

Hsu, H.-H., B. J. Hoskins, and F.-F. Jin, 1990: The 1985/86 intraseasonal oscillation and the role of the extratropics. *J. Atmos. Sci.,* **47,** 823–839.

Itoh, H., and M. Ghil, 1988: The generation mechanisms of mixed Rossby–gravity waves in the equatorial troposphere. *J. Atmos. Sci.,* **45,** 595–604.

Kuo, H. L., 1965: On formation and intensification of the tropical cyclones through latent heat release by cumulus convection. *J. Atmos. Sci.,* **22,** 40–63.

——, 1974: Further studies of the parameterization of the effect of cumulus convection on large-scale flow. *J. Atmos. Sci.,* **31,** 1232–1240.

Lau, N.-C., I. M. Held, and J. D. Neelin, 1988: The Madden–Julian oscillation in an idealized general circulation model. *J. Atmos. Sci.,* **43,** 3810–3832.

Manabe, S., J. S. Smagorinsky, and R. F. Strickler, 1965: Simulated climatology of a general circulation model with a hydrological cycle. *Mon. Wea. Rev.,* **93,** 769–798.

Matsuno, T., 1966: Quasi-geostrophic motions in the equatorial area. *J. Meteor. Soc. Japan,* **44,** 25–43.

Neelin, J. D., and J.-Y. Yu, 1994: Modes of tropical variability under convective adjustment and the Madden–Julian Oscillation. Part I: Analytical theory. *J. Atmos. Sci.,* **51,** 1876–1894.

——, I. M. Held, and K. H. Cook, 1987: Evaporation–wind feedback and low-frequency variability in the tropical atmosphere. *J. Atmos. Sci.,* **44,** 2341–2348.

Randall, D. A., and J. Wang, 1992: The moist available energy of a conditionally unstable atmosphere. *J. Atmos. Sci.,* **49,** 240–255.

Stark, T. E., 1976: Wave–CISK and cumulus parameterization. *J. Atmos. Sci.,* **33,** 2383–2391.

Webster, P. J., 1981: Mechanisms determining the atmospheric response to sea surface temperature anomalies. *J. Atmos. Sci.,* **38,** 554–571.

——, and J. R. Holton, 1982: Cross-equatorial response to middle-latitude forcing in a zonally varying basic state. *J. Atmos. Sci.,* **39,** 722–733.

Xu, K.-M., and K. A. Emanuel, 1989: Is the tropical atmosphere conditionally unstable? *Mon. Wea. Rev.,* **117,** 1471–1479.

——, A. Arakawa, and S. K. Krueger, 1992: The macroscopic behavior of cumulus ensembles simulated by a cumulus ensemble model. *J. Atmos. Sci.,* **49,** 2402–2420.

Yanai, M., and M.-M. Lu, 1983: Equatorially trapped waves at the 200 mb level and their association with meridional convergence of wave energy flux. *J. Atmos. Sci.,* **40,** 2785–2803.

——, S. Esbensen, and J.-H. Chu, 1973: Determination of bulk properties of tropical cloud clusters from large-scale heat and moisture budgets. *J. Atmos. Sci.,* **30,** 611–627.

Zhang, C., 1992: Laterally forced equatorial perturbations in a linear model. Part II: Mobile forcing. *J. Atmos. Sci.,* **50,** 807–821.

——, and P. J. Webster, 1992: Laterally forced equatorial perturbations in a linear model. Part I: Stationary transient forcing. *J. Atmos. Sci.,* **49,** 585–607.